ERROR ANALYSIS OF A MOBILE TERRESTRIAL LiDAR SYSTEM

M. Leslar[a], B. Hu[a], J.G. Wang[a]

[a]Department of Earth and Space Science and Engineering, Lassonde School of Engineering, York University, Toronto, Canada

The understanding of the effects of error on Mobile Terrestrial LiDAR (MTL) point clouds has not increased with their popularity. In this study, comprehensive error analyses based on error propagation theory and global sensitivity study were carried out to quantitatively describe the effects of various error sources in a MTL system on the point cloud. Two scenarios were envisioned; the first using the uncertainties for measurement and calibration variables that are normally expected for MTL systems as they exist today, and the second using an ideal situation where measurement and calibration values have been well adjusted. It was found that the highest proportion of error in the point cloud can be attributed to the boresight and lever arm parameters for MTL systems calibrated using non-rigours methods. In particular, under a loosely controlled error condition, the LiDAR to INS Z lever arm and the LiDAR to INS roll angle contributed more error in the output point cloud than any other parameter, including the INS position. Under tightly controlled error conditions, the INS position became the dominant source of error in the point cloud. In addition, conditional variance analysis has shown that the majority of the error in a point cloud can be attributed to the individual variables. Errors caused by the interactions between the diverse variables are minimal and can be regarded as insignificant.

La compréhension des effets des erreurs sur les nuages de points du LiDAR terrestre mobile (MTL) n'a pas augmenté avec sa popularité. Dans le présent article, nous avons effectué des analyses globales des erreurs fondées sur la théorie de propagation des erreurs et une étude globale de la sensibilité dans le but de décrire quantitativement les effets, sur le nuage de points, de diverses sources d'erreurs dans un système MTL. Nous avons envisagé deux scénarios, le premier utilisant les incertitudes dans les variables de mesure et de calibration qui sont normalement attendues pour les systèmes MTL qui existent actuellement et le second utilisant une situation idéale où les valeurs de mesure et de calibration ont été bien ajustées. Il a été établi que la proportion la plus élevée d'erreurs dans le nuage de points peut être attribuée aux paramètres de visée et de levier pour les systèmes MTL calibrés en utilisant des méthodes non rigoureuses. Plus particulièrement, dans une condition d'erreurs mal contrôlées, le levier entre le LiDAR et l'axe Z du INS (système de navigation par inertie) et l'angle de roulis entre le LiDAR et l'INS ont contribué à des erreurs plus grandes dans le nuage de points résultant que tout autre paramètre, y compris la position du INS. Dans des conditions d'erreurs fortement contrôlées, la position du INS est devenue la principale source d'erreurs dans le nuage de points. De plus, l'analyse de la variance conditionnelle a démontré que la majorité des erreurs dans un nuage de points peut être attribuée aux variables individuelles. Les erreurs causées par les interactions entre les diverses variables sont minimes et peuvent être considérées comme négligeables.

M. Leslar
mikel@optech.ca

B. Hu

J.G. Wang

Introduction

Achieving high accuracy surveys using Mobile Terrestrial LiDAR (MTL) systems is a challenge faced by many surveyors. Many factors contribute to the outcome of the final product, from base station locations and local GPS conditions to MTL system calibration and LiDAR measurement capabilities. In fact, the accuracy of an MTL survey can greatly depend on factors as variable as the weather. Controlling as many of these factors as possible would seem to be called for; however, too much attention and care in collecting the data can become costly in both time and money. A surveyor therefore

dx.doi.org/10.5623/cig2014-303 GEOMATICA Vol. 68, No. 3, 2014, pp. 183 to 194

needs to know what factors to spend time and effort controlling and by how much they should be controlled. A balance between controlling the error sources and producing results, as always, must be struck.

An MTL system usually consists of a LiDAR sensor integrated with an Inertial Navigation System (INS). The parameters used to convert raw MTL data into a georeferenced point cloud include both fixed parameters and measurements. The fixed parameters include the LiDAR calibration, the boresight and lever arms between the LiDAR and the INS. The measurements made by the MTL system include the position and orientation determined by the INS and the angles and ranges measured by the LiDAR. Some measurements are external to the MTL system, such as those made at the GPS base station, while others are confined to the moving platform on which the MTL system operates. This paper will focus on the error sources contained within the MTL system, specifically the measurement sources used to produce a point cloud and the errors that occur because of the integration of these measurements.

The calibration and measurement sources used in MTL are similar to those used by Mobile Airborne LiDAR (MAL). Similar to MTL, MAL collects INS positions and orientations and combines them with raw angles and ranges measured by the LiDAR. MAL also requires boresight and lever parameters between the LiDAR and INS to be determined. Unlike MAL, MTL is far more immersed in the target scene. This means that, generally, MTL systems have a larger range of possible boresight parameters between systems, the field of view of the LiDAR is much larger, and the ranges are generally much shorter.

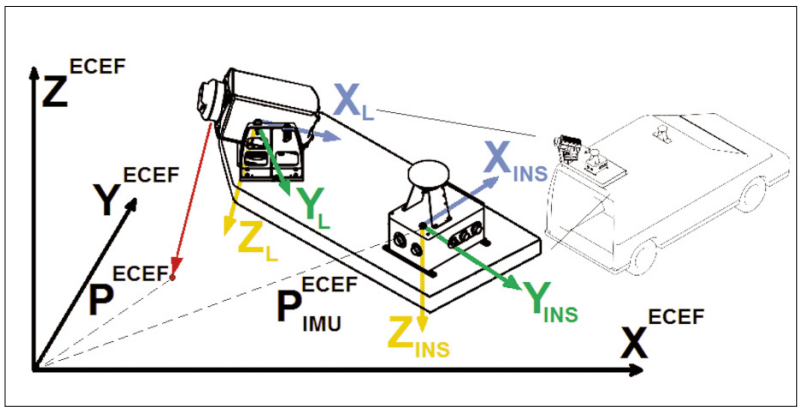

Figure 1: A typical configuration of a mobile terrestrial system plotted in the Earth Centered Earth Fixed (ECEF) coordinate system.

Measurements for the position and orientation of the MTL system are generated by the INS for any time t along the vehicle's path. The INS usually provides estimates of the errors for these position and orientation measurements. These error estimates are calculated in real time by the INS and are usually given in the form of root mean square (RMS) errors or one sigma standard deviations (σ), depending on the INS system in question. On the other hand, the measurements made by the LiDAR provide information on the location of any point p in range of the system. It is usual for the LiDAR to have fixed error quantities determined by the manufacturer or the surveyor in a controlled environment. These error estimates are almost always given as one sigma standard deviations. Many of these techniques have been well documented in static LiDAR systems [*Reshetyuk* 2009].

The errors associated with the integration of the LiDAR with the INS are usually the least understood and generally the hardest to quantify. While multiple methods have been proposed for LiDAR to IMU boresighting, few offer a reliable or rigorous approach for determining error. The documented methods for determining sensor to INS calibration parameters include manual visual methods [*Optech Inc.* 2008], software assisted visual methods [*Hypack Inc.* 2007; *Reson B.V.* 2011; *Virtual Geomatics Inc.* 2010; *Jeeninga* 2012; *Dix et al.* 2011] and algorithm based methods [*Rieger et al.* 2010; *Picard et al.* 2012; *Chan et al.* 2013]. Only the algorithm-based methods really give a means for determining error estimates for the LiDAR to INS calibration parameters.

Some work has already been done to analyze the errors inherent in MTL systems. Sources, such as *Alshawa et al.* [2007], *Glennie* [2007a], *Glennie* [2009], *Glennie* [2007b], discuss current works on the development of an error model for MTL systems that incorporate modified static terrestrial LiDAR systems in their design. In addition, overall performance data with respect to a control field can be found in *Leslar* [2009].

Despite the work that has already been published, the error sources for MTL remain under-analyzed. A comprehensive study of error sources involved with MTL systems is needed to understand and identify which factors can be better controlled for the purpose of producing high accuracy MTL point clouds. This paper presents the results of a comprehensive error analysis conducted on data collected with the Lynx Mobile Mapper [*Optech Inc.* 2008]. The Lynx system lends

itself to this type of testing since the calibration numbers are provided by the manufacturer in ASCII text file format. Unlike some other systems, where the calibration is stored in proprietary binary formats, the Lynx calibration values are open to the end user.

The Mathematical Models

The LiDAR Equation

Mobile LiDAR systems consist of two distinct components, the INS and the laser ranging system, as shown by a typical system configuration in Figure 1. As shown in Figure 1, the coordinates of point p in the Earth Centered and Earth Fixed (ECEF) coordinate system P^{ECEF} are a function of the laser range vector, the relative location and orientation of the LiDAR sensor to the INS system and the position and orientation of the INS. The base equation of this relationship can be expressed by Equation 1.

$$P^{ECEF} = P_{INS}^{ECEF} + L_{INS-LiDAR}^{ECEF} + L_{LiDAR-p}^{ECEF} \quad (1)$$

In Equation 1, P_{INS}^{ECEF} is the position of the INS, $L_{INS-LiDAR}^{ECEF}$ is the vector from the INS to the LiDAR sensor, and $L_{LiDAR-p}^{ECEF}$ is the vector from the LiDAR to the target point p. $L_{INS-LiDAR}^{ECEF}$ and $L_{LiDAR-p}^{ECEF}$ can be further deconstructed, as expressed in Equations 2 and 3.

$$L_{INS-LiDAR}^{ECEF} = R_1(B,L) \cdot R_2(r,p,h) \cdot l_{LiDAR}^{INS}(l_X, l_Y, l_Z) \quad (2)$$

$$L_{LiDAR-p}^{ECEF} = R_1(B,L) \cdot R_2(r,p,h) \cdot R_3(\theta_X, \theta_Y, \theta Z) \cdot l_p^{LiDAR}(\alpha, \beta, d, K \quad (3)$$

where l_{LiDAR}^{INS} is the lever arm vector from the INS body frame to the LiDAR body frame, l_p^{LiDAR} is the laser range vector between the LiDAR and the target point p, R_1 is the rotation matrix between the local geodetic coordinates and the ECEF coordinate frame, R_2 is the rotation matrix between the INS body frame and the local geodetic frame, and R_3 is the rotation matrix between LiDAR body frame and the INS body frame. The vectors l_{LiDAR}^{INS}, l_p^{LiDAR} and the matrices R_1, R_2, R_3 are themselves products of various measurements. We can group these measurements based on their dependencies. Group 1 consists of the INS position in Cartesian ECEF coordinates $\left(X_{INS}^{ECEF}, Y_{INS}^{ECEF}, Z_{INS}^{ECEF}\right)$. The Group 1 parameters are converted from the geodetic latitude (B), longitude (L) and ellipsoidal height (h) measured by the INS. Group 2 consists of *r, p, h,* which represent the roll, pitch and heading of the INS with respect to the local geodetic coordinate frame. Group 3 consists of l_X, l_Y, l_Z, which represent the components of the lever arm vector between the INS and the LiDAR. Group 4 consists of $\theta_X, \theta_Y, \theta_Z$, which represent the x, y and z rotations of the LiDAR coordinate frame in the INS frame. Group 5 consists of the LiDAR measurements, where α represents the horizontal angle measured by the LiDAR in the LiDAR body frame, β represents the vertical angle measured by the LiDAR in the LiDAR body frame, d represents the distance measured by the LiDAR to the target point p and K represents the zero error of the LiDAR instrument.

Each of the 18 aforementioned variables have an associated error estimate, usually in the form of an RMS or standard deviation. It is usual to assume that each of the measurements is normally distributed and that the RMS values reported by the INS can be considered equal to one sigma standard deviations (σ). These 18 standard deviations can be assigned to the same groups previously discussed.

Error Propagation Analysis

The error propagation analysis is a standard technique used to estimate errors in calculated values propagated from the errors of the measured parameters based on a known relationship. The equations for linear error propagation are fairly well understood and used across many disciplines [*Glennie* 2007b; *Goulden* 2009; *Tellinghuisen* 2001]. Performing linear error propagation first requires the non-linear equation presented in Equation 1 to be linearized as shown in Equation 4.

$$P^{ECEF} \approx P_0^{ECEF} + \frac{dP^{ECEF}}{dX_{INS}^{ECEF}} \cdot \Delta X_{INS}^{ECEF}$$

$$+ \frac{dP^{ECEF}}{dY_{INS}^{ECEF}} \cdot \Delta Y_{INS}^{ECEF} + \frac{dP^{ECEF}}{dZ_{INS}^{ECEF}} \cdot \Delta Z_{INS}^{ECEF}$$

$$+ \frac{dP^{ECEF}}{dB} \cdot \Delta B + \frac{dP^{ECEF}}{dL} \cdot \Delta L$$

$$+ \frac{dP^{ECEF}}{dr} \cdot \Delta r + \frac{dP^{ECEF}}{dp} \cdot \Delta p + \frac{dP^{ECEF}}{dh} \cdot \Delta h$$

$$+ \frac{dP^{ECEF}}{dlx} \cdot \Delta lx + \frac{dP^{ECEF}}{dly} \cdot \Delta ly + \frac{dP^{ECEF}}{dlz} \cdot \Delta lz$$

$$+ \frac{dP^{ECEF}}{d\theta_X} \cdot \Delta\theta_X + \frac{dP^{ECEF}}{d\theta_Y} \cdot \Delta\theta_Y + \frac{dP^{ECEF}}{d\theta_Z} \cdot \Delta\theta_Z$$

$$+ \frac{dP^{ECEF}}{d\alpha} \cdot \Delta\alpha + \frac{dP^{ECEF}}{d\beta} \cdot \Delta\beta + \frac{dP^{ECEF}}{dd} \cdot \Delta d$$

$$+ \frac{dP^{ECEF}}{dK} \cdot \Delta K \qquad (4)$$

In Equation 4, P_0^{ECEF} represents Equation 1 evaluated at the initial approximate variables $\left(X_{INS}^{ECEF(0)},\ Y_{INS}^{ECEF(0)},\ Z_{INS}^{ECEF(0)},\ B^0,\ L^0,\ r^0,\ p^0,\ h^0,\ l_X^0,\ l_Y^0,\ l_Z^0,\ \theta_X^0,\ \theta_Y^0,\ \theta_Z^0,\ \alpha^0,\ \beta^0,\ d^0,\ K^0\right)$ for the 18 measurements previously identified. Using the first derivatives from Equation 4, evaluated at each component (X, Y, Z) of the ECEF position, the design matrix (U) for a least square adjustment may be formed as shown in Equation 5.

$$U = \begin{bmatrix} \frac{dP^{ECEF}}{dX_{INS}^{ECEF}}_X & \frac{dP^{ECEF}}{dX_{INS}^{ECEF}}_Y & \frac{dP^{ECEF}}{dX_{INS}^{ECEF}}_Z \\ \vdots & \vdots & \vdots \\ \frac{dP^{ECEF}}{dK}_X & \frac{dP^{ECEF}}{dK}_Y & \frac{dP^{ECEF}}{dK}_Z \end{bmatrix} \qquad (5)$$

Using the additional information provided from the individual error estimates of the 18 input parameters and assuming no correlation between these variables, the variance-covariance matrix (Q) may be formed as shown in Equation 6.

$$Q = \begin{bmatrix} \sigma^2_{X_{INS}^{ECEF}} & 0 & \cdots & 0 \\ 0 & & \ddots & \vdots \\ \vdots & & & 0 \\ 0 & \cdots & 0 & \sigma_K^2 \end{bmatrix} \qquad (6)$$

This allows us to form the error propagation model shown in Equation 7.

$$\sigma^2_{P^{ECEF}} = U \cdot Q^{-1} \cdot U^T \qquad (7)$$

Conditional Variance Analysis

Conditional variance analysis is a method of global sensitivity analysis. Global sensitivity analysis is primarily used to study how the uncertainty in the output of a model can be apportioned to different sources of uncertainty in the model inputs [*Saltelli et al.* 2008]. First order sensitivity indices are a quantitative measure of the importance of the input variables on the calculated results. They apply to additive models. The more sensitive the calculated results are to small variances in any particular input variable, the greater the first order sensitivity index. The total effect indices are also a quantitative measure of the importance of the input variables on the calculated results. Unlike first order indices, however, they are applicable to all types of models independent of their model characteristics [*Schwieger* 2004].

Performing conditional variance analysis involves rewriting the terms of Equation 1 in terms of generic variables; Equation 1 can be expressed as shown in Equation 8.

$$P^{ECEF} = f\left(\cdots\ X_i\ \cdots\right) \text{ for } 1 \le i \le 18 \qquad (8)$$

Variance-based sensitivity analysis is carried out using simulated values for each variable (X_i). To acquire these simulated values one must generate N

random samples according to a specific probability density function for each of the variables [*Glen and Isaacs* 2012; *Bowyer and Danson* 2004]. Starting with the estimated values and their estimated standard deviations that we have for the 18 variables, these random samples can be generated based on the normal distribution.

Holding variable (X_i) fixed at the mean value of its randomly generated samples, while allowing the other variables to vary, N random values can be generated from Equation 8. The variance of the outputs of Equation 8 $\left(V\left(P^{ECEF}\middle|X_i\right)\right)$ can be calculated. If we then average this variance over all possible values of X_i we get the expectation of the variance, $E\left(V\left(P^{ECEF}\middle|X_i\right)\right)$. Based on linear algebra we can compute the main effect of X_i on $P^{ECEF}\left(V\left(E\left(P^{ECEF}\middle|X_i\right)\right)\right)$ from Equation 9 [*Saltelli et al.* 2008].

$$V\left(P^{ECEF}\right)=E\left(V\left(P^{ECEF}\middle|X_i\right)\right)+V\left(E\left(P^{ECEF}\middle|X_i\right)\right) \tag{9}$$

The larger $V\left(E\left(P^{ECEF}\middle|X_i\right)\right)$ is, the more influential X_i is on the output of Equation 8. Therefore, from the relationship shown in Equation 9, the first order Sobol index for the variable X_i can be computed according to Equation 10 [*Saltelli et al.* 2008].

$$S_i=\frac{V\left(E\left(P^{ECEF}\middle|X_i\right)\right)}{V\left(P^{ECEF}\right)} \tag{10}$$

Higher order indices are computed by holding more than one variable fixed as shown in Equation 11 [*Saltelli et al.* 2008].

$$S_{i,j,k,\cdots}=\frac{V\left(E\left(P^{ECEF}\middle|X_i,X_j,X_k,\cdots\right)\right)}{V\left(P^{ECEF}\right)}-S_i-S_j-S_k\cdots \tag{11}$$

Computing all the higher order terms becomes inefficient due to the large number of combinations for models with a large number of variables. For example, the 18 variables in Equation 1 will generate 48,620 9th order Sobol indices alone. It is therefore desirable to calculate the total effect for a variable $\left(S_{t_i}\right)$. This can be done by calculating the variance of the expected values when all the variables in the model are held fixed while allowing only X_i to vary $\left(V\left(E\left(P^{ECEF}\middle|X_{\sim i}\right)\right)\right)$. The total effect can be computed as shown in Equation 12 [*Saltelli et al.* 2008].

$$S_{t_i}=1-\frac{V\left(E\left(P^{ECEF}\middle|X_{\sim i}\right)\right)}{V\left(P^{ECEF}\right)} \tag{12}$$

For additive models $\sum_{i=1}^{n}S_i=1,\ \ S_{t_i}=S_i$

For non-additive models $S_{t_i}>S_i$

Implementation and Testing

The error propagation described above was implemented in Microsoft Visual C++ 6.0 and the conditional variance analysis was implemented in Matlab R14. For testing purposes, MTL data were collected using the Lynx Mobile Mapper. These data were collected in a mostly empty parking lot to allow the LiDAR to reach its maximum range. The data used is shown in Figure 2.

The northern section of the data contains a tree line that is located approximately 50 m from the

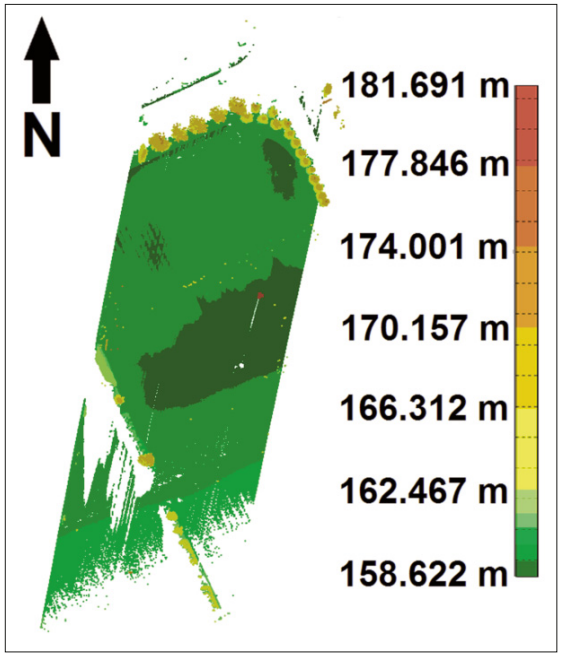

Figure 2: Lynx data collected in a parking lot in Vaughan, Ontario, Canada, on May 19, 2012. The colour scale indicates the height above the WGS84 ellipsoid.

LiDAR sensor; the southern section of the data contains an open parking lot with some hedges and a lamp post. A building and two cars exist in the parking lot at long range for the LiDAR sensor. They are not seen in Figure 2 as they are at extreme long range for the LIDAR system, but random shots were collected off of them.

To analyze the effect of errors in the 18 parameters on the output point cloud, it is first necessary to collect the error estimates for each parameter. The error estimates concerning the position and orientation of the Lynx system in the ECEF mapping frame are generated in real time by the INS. In the case of the Lynx system, the INS used is an Applanix POS.

Out of the five variables related to the position of the INS, it was found that the latitude and longitude contribute less than a millimetre of error to the final solution. For the purposes of testing, they were therefore excluded from further consideration since their contribution to the overall error is insignificant. The LiDAR errors are published by Optech, the manufacturer of the Lynx sensor head. They state that the one sigma range accuracy of the LiDAR is 0.008 m. Examining planar surfaces in multiple points taken by the Lynx system reveals that the range accuracy of the system is generally better than this, usually around 0.003 m. Therefore these numbers will be compared to see the effect of each.

That leaves the six errors associated with the integration of the LiDAR and INS system, the so-called boresight and lever arm parameters. Typically, boresight operation for many MTL and multibeam sonar systems is done using non-rigours methods such as the so-called "Patch Test" [*Hypack Inc.* 2007]. Multiple manufacturers of this equipment and the software used to process the data use these methods for determining boresight parameters for MTL [*Optech Inc.* 2008; *Hypack Inc.* 2007; *Reson B.V.* 2011; *Virtual Geomatics Inc.* 2010; *Jeeninga* 2012; *Dix et al.* 2011]. Table 1 gives a breakdown of these parameters, their groups, expected error values and the ideal error values for these parameters obtained by accurate calibrations.

Some literature sources agree that the expected lever arm uncertainties listed in Table 1 are typical for most systems [*Glennie* 2007b]. However, the same source indicates that the typical manual boresight method should facilitate an uncertainty of 0.005° for roll and pitch and 0.008° for heading [*Glennie* 2007b]. The same source further states

Table 1: Expected and ideal uncertainties in MTL parameters.

Parameter	Group	Expected	Ideal
$\sigma_{X_{INS}^{ECEF}}$, Position X [m]	1	Estimated from INS	Estimated from INS
$\sigma_{Y_{INS}^{ECEF}}$, Position Y [m]	1	Estimated from INS	Estimated from INS
$\sigma_{Z_{INS}^{ECEF}}$, Position Z [m]	1	Estimated from INS	Estimated from INS
σ_r, Platform Roll [degrees]	2	Estimated from INS	Estimated from INS
σ_p, Platform Pitch [degrees]	2	Estimated from INS	Estimated from INS
σ_h, Platform Heading [degrees]	2	Estimated from INS	Estimated from INS
σ_{lx}, LiDAR X Lever Arm [m]	3	0.02	0.004
σ_{ly}, LiDAR Y Lever Arm [m]	3	0.02	0.004
σ_{lz}, LiDAR Z Lever Arm [m]	3	0.02	0.004
σ_{θ_X}, LiDAR Roll [degrees]	4	0.02	0.001
σ_{θ_Y}, LiDAR Pitch [degrees]	4	0.02	0.001
σ_{θ_Z}, LiDAR Heading [degrees]	4	0.02	0.001
σ_a, LiDAR Horizontal Angle [degrees]	5	0.0055	0.0055
σ_β, LiDAR Vertical Angle [degrees]	5	0.0055	0.0055
σ_d, LiDAR Distance [m]	5	0.008	0.003
σ_K, LiDAR Zero Error [m]	5	0.01	0.005

that the expected results from a least squares adjustment should have a typical uncertainty of 0.001° for roll and pitch and 0.004° for heading.

The values from the manual boresight seem optimistic. When performing a manual boresight, a more likely value for the boresight roll, pitch and heading uncertainty is 0.02°, as reflected in Table 1.

Results and Discussion

The Lynx data was run through the error propagation model for both the expected error estimates and the ideal error estimates. The results were converted to a colour scale and applied to the point cloud. The results from the error propagation analysis for the expected error estimates are shown in Figure 3.

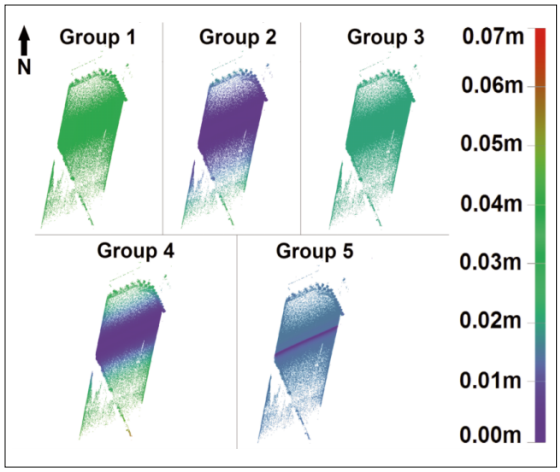

Figure 3: Results of linear error propagation using the expected error estimates. Each of the five identified groups of variables was isolated and the error propagation performed.

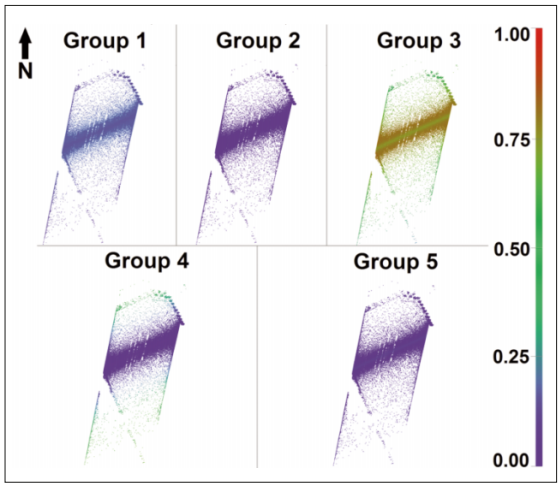

Figure 4: Results of first order conditional variance analysis using the expected error estimates. Each of the five identified groups of variables was isolated and the Sobol indices computed.

The colour scales applied to the point clouds in Figure 3 show that the largest source of error in the resultant point cloud is consistently caused by the INS positional errors. The poor quality of the lever arm estimates in this case makes the lever arms between the LiDAR and the INS the second most consistent source of error in the system. The angular errors from the INS orientation variables, as well as the LiDAR to INS boresight variables, take on increasing significance as the range from the LiDAR sensor increases. The LiDAR measurements themselves comprise the least source of error in the point cloud.

The colour-mapped data from the first order conditional variance analysis for the expected error estimates are shown in Figure 4. The colour maps in Figure 4 show that when the expected error estimates exist in the point cloud, the largest proportion of the error in the MTL point cloud is given by the LiDAR to INS lever arm values in Group 3. The rotations between LiDAR coordinate frame and the INS coordinate frame (Group 4) in turn take on increasing significance as the range from the LiDAR sensor increases.

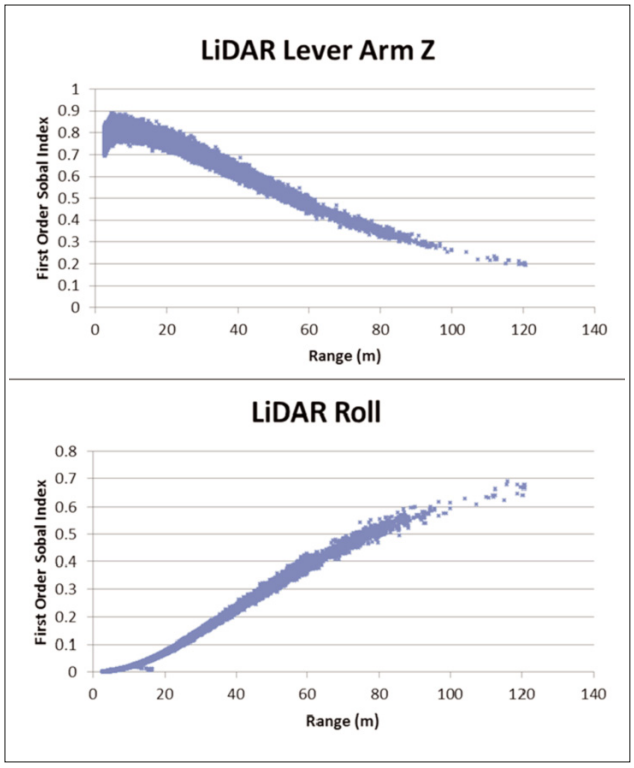

Figure 5: Scatter plots of the first order Sobol indices for Z lever arm and boresight roll in Lynx Mobile Mapper data.

Since the color maps in Figure 4 refer to groups of variables instead of individual variables, the Sobol indices for each variable were calculated. It was found that the lever arm almost exclusively responsible for this result is the Z lever arm. The scatter plots in Figure 5 show that at close ranges the Z lever arm from the LiDAR to INS contributes up to 90% of the error in the point cloud. Figure 5 also shows that as the range from the sensor increases, the significance of the Z lever arm tapers off and is replaced by the LiDAR to INS roll angle. At the maximum range of the LYNX sensor, the effect of roll under these conditions becomes the single most significant source of error in the point cloud. Figure 5 shows that at the maximum range of the Lynx sensor, the error generated by the LiDAR to INS roll angle is upwards of 70%.

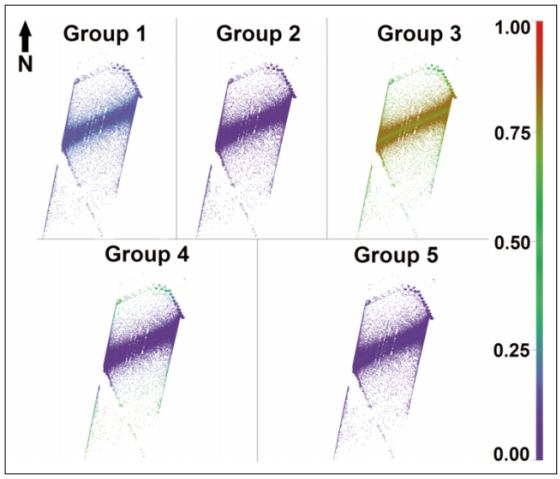

Figure 6: Results of the total effect conditional variance analysis using the expected error estimates. Each of the five identified groups of variables was isolated and the Sobol indices computed.

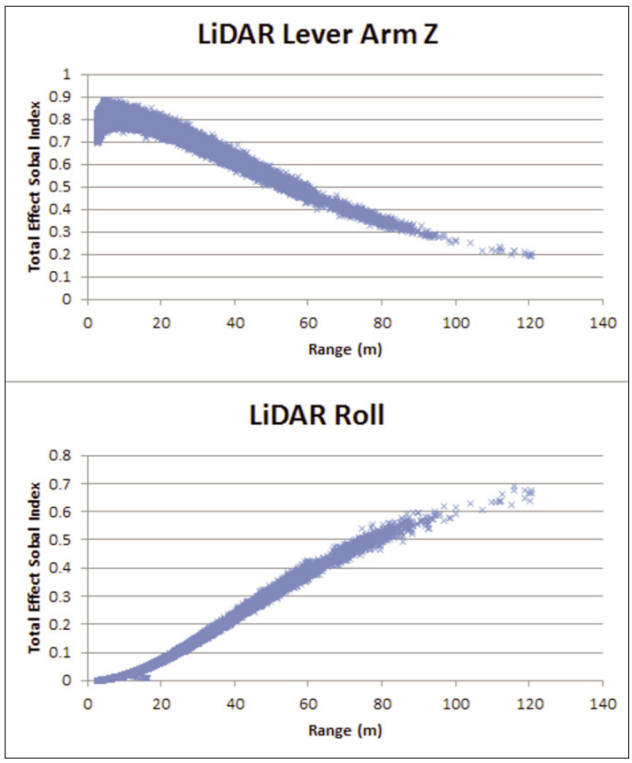

Figure 7: Scatter plots of the total effect Sobol indices for Z lever arm and boresight roll in Lynx Mobile Mapper data.

In addition to the first order indices of the conditional variance analysis, the total effect indices for the five groups were also computed. These total effect indices were converted to a colour scale and applied to the point cloud. Figure 6 shows the total effect indices for the expected error estimates. Figure 7 shows the two most important scatter plots of the total effect indices for the expected error estimates. The colour-mapped data in Figure 6 show that when the expected error estimates exist in the point cloud, the total effect indices from the conditional variance analysis are practically identical to the first order effect.

Breaking down the groups into individual variables as we did with the first order indices, again we see that the LiDAR to INS Z lever arm and the LiDAR to INS roll angle are the most significant parameters in terms of their proportional effect on the point cloud. The scatter plots shown in Figure 7 indicate that the LiDAR to INS Z lever arm contributes upwards of 90% of the error at ranges close to the LiDAR sensor and decreases as the range increases. Figure 7 also shows that the LiDAR to INS roll angle has little significance close to the LiDAR sensor, but makes up almost 70% of the error at maximum range.

For this MTL point cloud, error propagation with the expected error estimates (Figure 3) indicates that the largest source of error in the point cloud comes from the INS position. The first order conditional variance analysis tells a different story. Figure 4 indicates that the INS position only accounts for about 12% of the total error in the point cloud. The largest source of error is actually the LiDAR to INS lever arm, not the INS position. The fact that both Figures 5 and 7 show the Z-lever arm and the LiDAR to INS roll angle contributing upwards of 90% and 70% of the total error at various times highlights the significance of these two parameters. This was apparent from the error propagation model.

The fact that the first order sensitivity indices in Figure 4 add up to one, and that the first order indices closely mirror the total effect indices shown in Figure 6, indicates that Equation 1 is an additive model. This implies that the majority of the total

effect can be attributed to the individual variables, i.e., the first order effect. Cross-effects caused by the various variable combinations are minimal and can be regarded as insignificant. The higher order indices from Equation 11 can therefore be disregarded from further error analysis.

The results from the error propagation for the ideal error estimates are shown in Figure 8. Figure 8 shows that using the ideal error estimates, the error in the resulting point cloud will be heavily influenced by the errors inherent in the INS system. The most significant source of error in Figure 8 is in the INS position (Group 1) at a constant 3–4 cm. The second largest source of error according to Figure 8 is given by the INS orientation data (Group 2). This error is insignificant at the LiDAR and increases as the range from the LiDAR increases. The LiDAR to INS lever arms, the rotations of the LiDAR coordinate frame in the INS frame and the LiDAR measurements themselves are shown to contribute an insignificant amount of error in Figure 8.

The colour maps in Figure 9 show that when the ideal error estimates exist in the point cloud, the largest proportion of error in the MTL point cloud is given by the INS position parameters of Group 1. The LiDAR measurement parameters of Group 5 contribute the next highest percentage of error in the MTL point cloud, while the other groups disappear into insignificance.

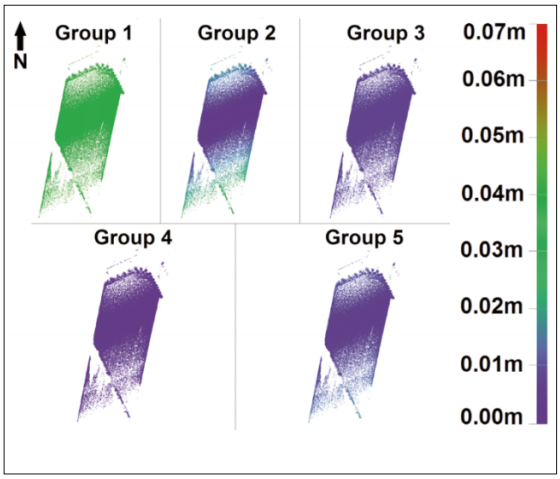

Figure 8: Results of linear error propagation using the ideal error estimates. Each of the five identified groups of variables was isolated and the error propagation performed.

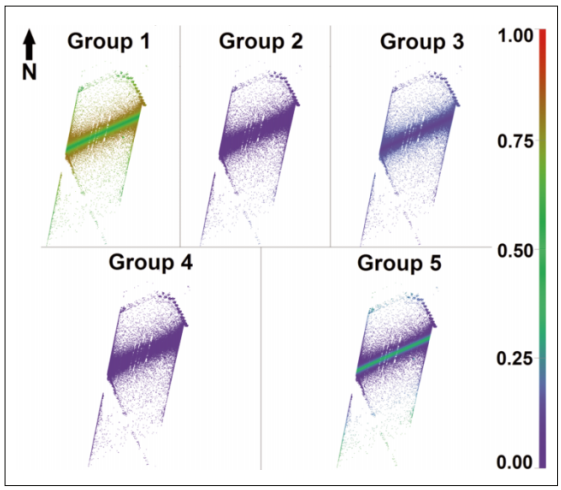

Figure 9: Results of first order conditional variance analysis using the ideal error estimates. Each of the five identified groups of variables was isolated and the Sobol indices computed.

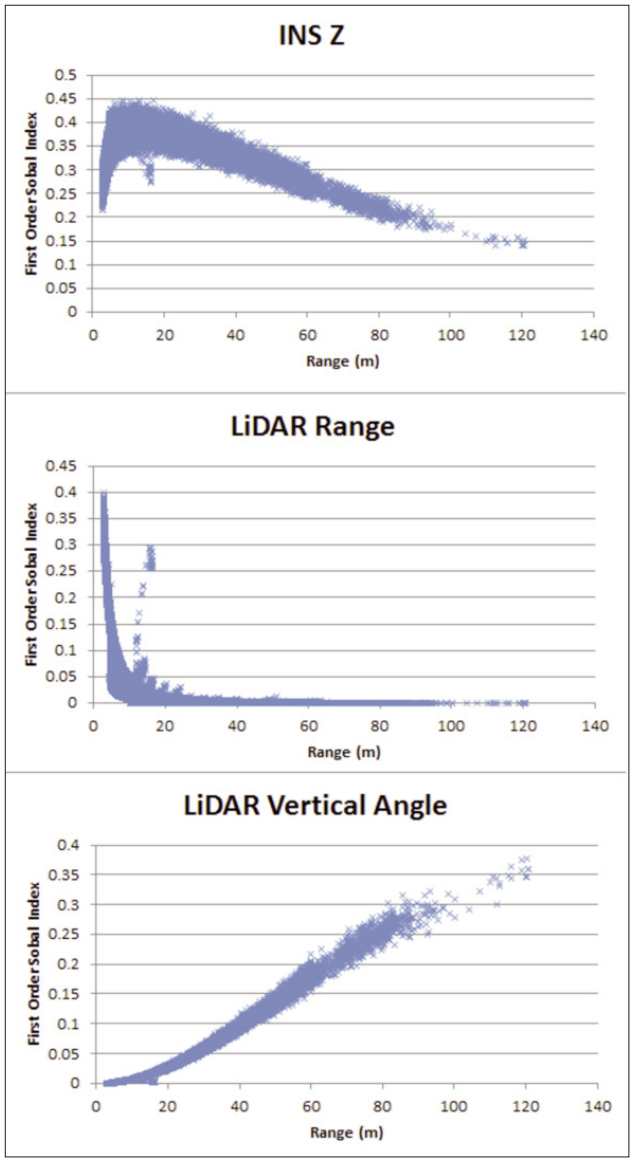

Figure 10: Scatter plots of the first order Sobol indices for Z coordinate of the INS position, the LiDAR range and the LiDAR measured vertical angle.

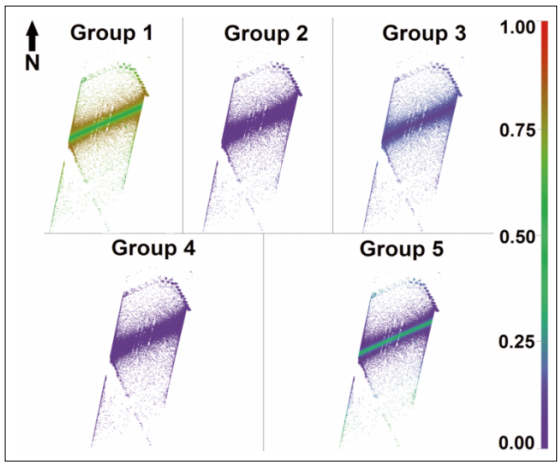

Figure 11: Results of total effect conditional variance analysis using the ideal error estimates. Each of the five identified groups of variables was isolated and the Sobol indices computed.

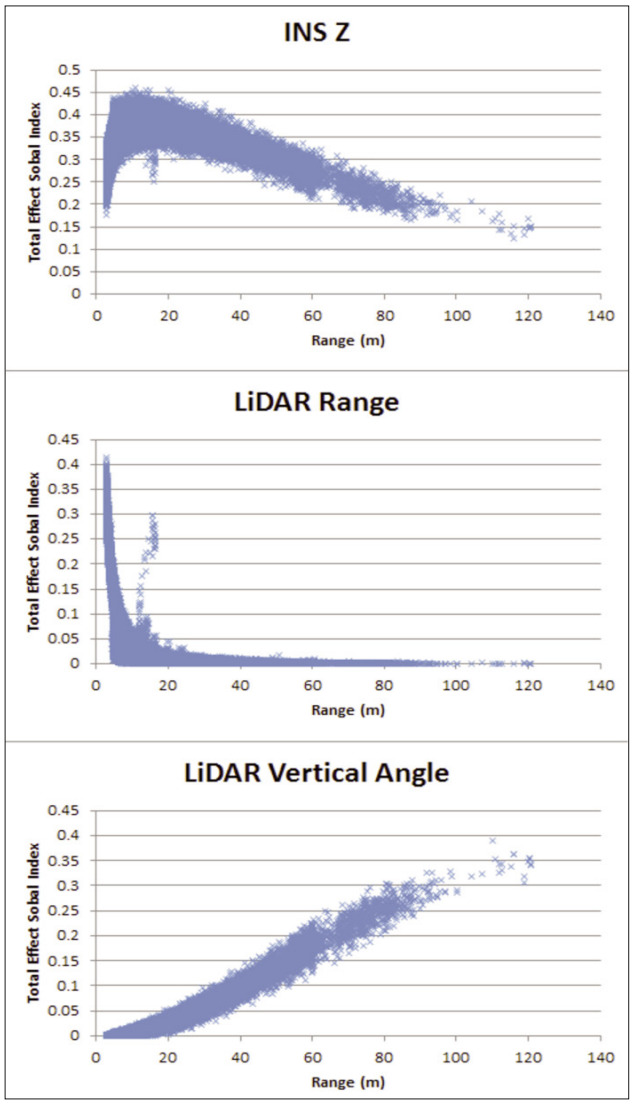

Figure 12: Scatter plots of the total effect Sobol indices for Z coordinate of the INS position, the LiDAR range and the LiDAR measured vertical angle.

The scatter plots for the ideal error estimates were calculated and it was found that the Z coordinate of the INS position, the LiDAR range and the LiDAR vertical angle were the most significant. Figure 10 shows that the Z coordinate from the INS contributes up to 45% of the total error at close ranges under ideal error conditions. The LiDAR range contributes another 40% of the error at these same ranges. In some spots where laser saturations occur, spikes can be seen in the LiDAR range scatter plot in Figure 10; however, the general trend of the data is for the laser range to contribute less error to the overall solution as range increases. As the significance of the LiDAR range decreases, the vertical angle of the LiDAR takes over as the major source of error from the LiDAR, peaking at around 40% at long ranges.

The colour-mapped data in Figure 11 show that when the ideal error estimates exist in the point cloud, the total effect indices from the conditional variance analysis are also very similar to the first order effect. The INS position (Group 1) consistently contributes the largest proportion of error to the MTL point cloud, with the LiDAR measurements (Group 5) contributing the next largest proportion of error to the MTL point cloud. The other groups vanish into insignificance.

Looking at the total effect Sobol indices for the ideal case, we see similar results as those found with the first order Sobol indices. Figure 12 shows the total effect Sobol indices for the same parameters that were shown in Figure 10, namely, the Z coordinate of the INS position, the LiDAR range and the LiDAR vertical angle. As expected, the results for the total effect Sobol indices show results identical to the first order Sobol indices of Figure 10. Just as in Figure 10, Figure 12 shows that the INS Z coordinate contributes up to 45% of the overall error and that there is a reciprocal relationship between the amount of error contributed by the laser range finder and the LiDAR encoders.

Figures 9, 10, 11 and 12 reinforce the implication that the majority of the total effect can be attributed to the first order effect. The higher order effects from Equation 11 can therefore be treated as insignificant.

Contrasting the result obtained using the expected error estimates in the error propagation model, we see that the ideal error estimates in the error propagation model clearly give us the INS position as the main source of error in the point cloud (Figure 8). In Figure 8, these three groups of variables show error estimates less than 1 cm for all the points in the point cloud. Only the INS position and orientation errors play a significant role in the final point cloud error. The conditional variance

analysis bears this out, showing that the INS position errors make up more than 50% of the errors throughout the point cloud (Figure 9). Figure 9 shows that the INS orientation, LiDAR lever arms and the LiDAR boresight collectively make up a small percentage of the total error. We also see in Figure 9 that the second most significant source of error is from the LiDAR and that it occurs directly along the MTL system's path. This is due to effects in the LiDAR receiver caused by the extreme short ranges measured by the system. The rest of the error from the LiDAR increases as the range increases. This indicates that the angular uncertainties in the LIDAR's encoder combined with range and zero error uncertainties become more pronounced in the resulting point cloud at range.

Conclusions

The nature of error in MTL is still being discovered. While research into the nature of error generated by Airborne LiDAR systems has been conducted for several years, research into errors in MTL has just begun.

Conditional variance analysis has shown that the contribution by the interactions among the measured parameters to the variances of the points in an MTL point cloud is insignificant. The sizes of the variances for the measurements used to produce a point are the primary source of error in the output point cloud. In particular, under a loosely controlled error condition, the LiDAR to INS Z lever arm and the LiDAR to INS roll angle contributed more error in the output point cloud than any other parameter, including the INS position. Under tightly controlled error conditions, the INS position becomes the dominant source of error in the point cloud.

Therefore, MTL systems that have been mounted and boresighted using non-rigorous methodologies provide the greatest source of error in the resulting point cloud. It is therefore essential that high quality rigours methods be used to derive the integration parameters so that high quality LiDAR data may be collected with an MTL system.

References

Alshawa, M., E. Smigiel, P. Grussenmeyer, and T. Landes. 2007. Integration of a terrestrial LIDAR on a mobile mapping platform: first experiences. 5th International Symposium on Mobile Mapping Technology. Padua, Italy. 2007.

Bowyer, P. and F.M. Danson. 2004. Sensitivity of spectral reflectance to variation in live fuel moisture content at leaf and canopy level. *Remote Sensing of Environment.* 92: 297-308.

Chan, T., D. Lichti, and C. Glennie. 2013. Multi-feature based boresight self-calibration of a terrestrial mobile mapping system. *ISPRS Journal of Photogrammetry and Remote Sensing*. 82: 112-124.

Dix, M., A. Abd-Elrahman, B. Dewitt and L. Nash. 2011. Accuracy evaluation of terrestrial LiDAR and multibeam sonar systems mounted on a survey vessel. *J. Surv. Eng.* doi: 10.1061/(ASCE)SU.1943-5428.0000075

Glen, G. and K. Isaacs. 2012. Estimating Sobol sensitivity indices using correlations. *Environmental Modelling & Software.* 37: 157-166.

Glennie, C. 2007a. Reign of point clouds: a kinematic terrestrial LIDAR scanning system. *Inside GNSS Magazine.* 2(7), Fall 2007.

Glennie, C. 2007b. Rigorous 3D error analysis of kinematic scanning LIDAR systems. *Journal of Applied Geodesy.* 1(3): 147–157, November 2007. doi: 10.1515/jag.2007.017

Glennie, C. 2009. A kinematic terrestrial LIDAR scanning system. Proceedings of the Transportation Research Board 88th Annual Meeting, Washington D.C. January 11–15, 2009. Paper No. 09-0122.

Goulden, T. 2009. *Prediction of error due to terrain slope in LiDAR observations*. Thesis, MS in Geodesy and Geomatics. University of New Brunswick, 2009. Published as technical report No. 265, University of New Brunswick.

Hypack Incorporated. 2007. *Hysweep User's Manual*. Middletown, Connecticut, USA: 2007.

Jeeninga, B. 2012. Mobile laser calibration. Presentation given by QPS. Zeist: The Netherlands, 2012.

Leslar, M. 2009. Extraction of geo-spatial information from LiDAR-based mobile mapping system for crowd control planning. *IEEE Xplore Special Issue, Science and Technology for Humanity (TIC-STH)*. 2009 IEEE Toronto International Conference. 468-472.

Optech Incorporated. 2010. *Lynx Software Manual–Revision B*. Vaughan, Ontario, Canada: 2008.

Picard, A., T. Touze, N. Seube, J.G. Nistad, and M. Rondeau. 2012. Calibration of vessel mounted LiDAR. Proceedings of the Canadian Hydrographic Conference, May 15–17, 2012. Niagra Falls, Ontario, Canada.

Reshetyuk, Y. 2009. *Self-calibration and direct georeferencing in terrestrial laser scanning*. Thesis, PhD in Infrastructure Geodesy. Royal Institute of Technology, Department of Transport and Economics, Stockholm, Sweden.

Reson B.V. *PDS2000 Multibeam Office Training. PDS2000 v3.7*. Rotterdam: 2011.

Rieger, P., N. Studnicka, M. Pfennigbauer, and G. Zach. 2010. Boresight alignment method for mobile laser scanning systems. *Journal of Applied Geodesy*. 4(1): 13–21, June 2010. doi: 10.1515/jag.2010.002

Saltelli, A., M. Ratto, T. Andres, F. Campolongo, J. Cariboni, D. Gatelli, M. Saisana, and S. Tarantola.

2008. *Global sensitivity analysis. The Primer.* John Wiley & Sons, Ltd. 20-25.

Schwieger, V. 2004. Variance-based sensitivity analysis for model evaluation in engineering surveys. INGEO 2004 and FIG Regional Central and Eastern European Conference on Engineering Surveying. Bratislava, Slovakia, November 11–13, 2004.

Tellinghuisen, J. 2001. Statistical error propagation. *Journal of Physical Chemistry*. 105: 3917-3921.

Virtual Geomatics Incorporated. *LiDAR Calibrator*. Austin Texas USA: 2010.

Authors

Michael Leslar is a PhD candidate in the Geomatics Engineering Program, Department of Earth and Space Science and Engineering, Lassonde School of Engineering at York University, Toronto, Canada. He has a Bachelor's degree in Civil Engineering (Geomatics) and a Master's degree in Applied Science (Geomatics) from the Department of Civil Engineering at Ryerson University, Toronto, Canada. In addition to being a part time student, he has been a full time employee of Optech Incorporated for the last eight years. His current work and research interests focus on terrestrial LiDAR data processing, feature extraction, LiDAR sensor calibration, sources of error in terrestrial LiDAR and their correction.

Baoxin Hu received her Bachelor's and Master's degrees in Electrical Engineering from Tianjin University, Tianjin, China and PhD degree in Remote Sensing and GIS from Boston University, Boston, USA. She is currently an associate professor in Geomatics Engineering, York University, Toronto, Canada. Her research interests include 3D scene reconstruction from LiDAR and optical imagery and vegetation characterization from remotely sensed data.

Jian-Guo Wang is an Associate Lecturer in Geomatics Engineering, faculty member of Lassonde School of Engineering and Faculty of Graduate Studies of York University in Toronto, Canada. He obtained his Bachelor's and Master's Degrees in Surveying Engineering from Wuhan Technical University of Surveying and Mapping, Wuhan, China, and his Dr-Ing in Surveying Engineering from University of The Federal Armed Forces, Munich, Germany. His current research interests focus on multisensor integrated positioning and navigation technology, GNSS, mobile mapping, engineering surveying, and advanced data processing algorithms in geomatics. ❑